microscopy [1–4]. This is one of the reasons why colloids are interesting as model system for fundamental condensed matter physics. Another reason is that the interparticle potential can be modified relatively easily from, for example, short-range repulsive, or almost hard-sphere like, to long-range repulsive. However, until recently, no quantitative 3D real space measurements were reported for particles with interactions reaching further than the particle diameter. In a previous paper [4], we showed how sterically stabilized dispersions of polymethylmethacrylate (PMMA) spheres in a mixture of cyclohexyl bromide (CHB) and *cis*-decalin can be density and refractive index matched, and interact through electrostatic repulsions over distances larger than the particle size. Here we will show that for this model system the 3D radial distribution function (RDF) of the colloidal fluid can be determined. For the measurements presented in this paper, the interactions were well described by a density independent Yukawa, or exponentially screened Coulomb, potential. Under certain approximations, this potential can be derived from a solution of the Poisson–Boltzmann equation and forms the repulsive electrostatic part of the Derjaguin–Landau–Verwey–Overbeek (DLVO) potential [5]. The van der Waals forces, which are always attractive for similar particles and are also part of the DLVO potential, can be neglected for the rest of this paper. Firstly, because the refractive index of the particles is matched in the optical frequency range to that of the solvent mixture and secondly, because we will be only dealing with long-range potentials and very low salt concentrations. We found the parameters for the Yukawa potential by comparison with Monte Carlo (MC) computer simulations. We also confirmed experimentally and by comparison with computer simulations that the same potential gave a good description of the restoring force for particle displacements away from the lattice positions in a colloidal crystal, and that the potential was in agreement with the freezing volume fraction. The purely repulsive nature of the electrostatic part of the DLVO potential, which was only derived for interactions between two particles, and the pair-wise additivity assumed in the description of the structure of strongly interacting dispersions have been questioned in several experimental papers [6–10]. In particular Brunner *et al* [9] showed deviations from pair-wise additivity in a 2D system, which they believed should also apply in 3D. Our procedure probes pair-wise additivity for a 3D system in a similar way.

There has been a considerable theoretical effort to explain these observations (see, for a review, [11] and also [12–14]). Our new model system will provide a good test case for quite long-range interactions, as the background concentration of ions can be quite low: an order of magnitude less than in water, without ion exchange, $\sim 10^{-8}$ M. In the case that the interactions are larger than the particle diameter it is expected that the pair-wise additivity will break down [13, 14].

We determined the interparticle potential for a dispersion in which the screening length was determined by the background ion concentration of the CHB solvent. By conductivity and electrophoresis measurements, we will show that, by addition of the salt tetrabutylammonium chloride (TBAC), we can not only control the Debye screening length, but the particle surface charge can also be reduced and even its sign reversed.

Finally, we present preliminary observations of phenomena that were mostly transient, but had a lot of similarities to anomalous behaviour previously reported for strongly deionized systems in water [6–8]. We consider 'anomalous behaviour' as that which is not compatible with pair-wise additive repulsive potentials, based on the linear approximation to the Poisson–Boltzmann equation. The phenomena were extremely long-range repulsions incompatible with the concentration of background ions, 'coexistence' of high- and low-volume fraction crystals, and voids.

The paper is organized as follows. After giving experimental details, we first present the conductivity and electrophoresis measurements, then discuss the determination of the interaction potential for colloidal liquids and crystals at different volume fractions, and finally

we describe and discuss a possible reason for the anomalous 'phase' behaviour. We end with conclusions.

2. Experimental and computer simulation

2.1. Colloids and solvents

The polymethylmethacrylate (PMMA) particles used in this study were sterically stabilized with poly(12-hydroxystearic acid) and made by dispersion polymerization [15]. The particles were covalently labelled by the fluorophores 7-nitrobenzo-2-oxa-1,3-diazol (NBD) or rhodamine isothiocyanate (RITC) according to the procedure described by Bosma *et al* [16]. The PMMA particles labelled with NBD had a diameter of 2.00 μm and those labelled with RITC were 2.16 μm. Both types of particles had a polydispersity (relative width of the size distribution) of 3% as determined by light scattering and electron microscopy [16]. For the determination of the RDFs (section 3.2) the colloids were dispersed in a nearly density-matched mixture of cyclohexyl bromide (CHB, Sigma-Aldrich) and *cis*-decalin (Sigma-Aldrich). This mixture contained around 80% CHB and 20% *cis*-decalin by weight and also nearly matches the refractive index of the PMMA spheres. The CHB was washed with a 37% solution of HCl, a 5% solution of $NaHCO_3$ and deionized water, then dried with $CaCl_2$ and finally distilled under vacuum, in a similar way as before [4]. For the electrophoresis measurements the density matching was done using 12% by weight of hexane (Merck) in order to have enough refractive index contrast to use light scattering. For studies of the phase behaviour dispersions were made in pure CHB. In all cases, the particles were dispersed in the solvent after drying from petroleum ether under a nitrogen flush at room temperature. The dispersions studied with confocal microscopy were confined to glass capillaries with inner dimensions of 0.1 mm $\times$ 1.0 mm or 0.1 mm $\times$ 2.0 mm (VitroCom) and sealed at each end, either with Norland Optical adhesive no 68 (Norland Optical Products Inc.) or by melting.

The dispersion of NBD–PMMA spheres used for determination of the interaction potential from the RDF in the colloidal liquid and crystals had an initial volume fraction of 0.04 and was centrifuged at 1000 rpm (Hettich Zentrifugeren Rontina 46s) for 18 h to create a density gradient, and then laid horizontally for 24 h to allow the counter- and background-ions to equilibrate. No systematic change in colloid density was measured during the timescale of the data acquisition (up to 3 h), nor was any change in phase behaviour seen on a timescale of weeks.

The range of the repulsive interactions between the particles and the sign of the charge on the particles was tuned by adding the salt tetrabutylammonium chloride (TBAC, Sigma-Aldrich). Dilutions were made from a stock solution of TBAC in CHB, which was close to the saturation concentration at ambient temperature and pressure (260 μM).

2.2. Electrophoresis and conductivity measurements

Debye screening lengths, κ^{-1}, of our dispersions were estimated by applying Walden's rule to conductivity data. This rule states that the product of the limiting equivalent conductance and the viscosity is a constant between different media, i.e. $\Lambda\eta = \Lambda^0\eta^0$. For TBAC in water at 25 °C, $TBA^+\Lambda^0$ is 19.4 cm^2 S mol^{-1} and $Cl^-\Lambda^0$ is 76.3 cm^2 S mol^{-1}. Then, the ionic strength c_i equals $(10^3)\ K/\Lambda$, K being the measured electrical conductivity, and the Debye screening length is $\kappa^{-1} = 0.034(\varepsilon_r/c_i)^{1/2}$, where ε_r is the relative dielectric constant. The ratio c_i/c is the degree of dissociation of the ionic species, where c is the salt concentration. We only give conductivities and Debye screening lengths in the pure CHB solvent, as exact viscosities and

dielectric constants of the solvent mixtures were not known. The conductometer (Radiometer Copenhagen) operated at 586 Hz and was connected to a three-pole flow cell. The conductivity of the purified CHB was 0.002 μS cm^{-1}, close to the limit of the instrument resolution. Apart from the pure solvent we mainly used a CHB–hexane mixture containing 40 μM TBAC for the electrophoresis measurements. The conductivity of a 40 μM TBAC solution in CHB amounted to 0.045 μS cm^{-1}, implying a degree of dissociation of 0.027.

To quantify the charge on the particles electrophoretic light scattering measurements were performed (Coulter Delsa 440SX). As mentioned above, dilute dispersions of both the NBD- and RITC-labelled particles were made in a density-matched mixture of CHB and hexane to prevent sedimentation and to get sufficient scattering. The phase behaviour in this mixture was similar to that in density-matched mixtures of CHB with *cis*-decalin and in pure CHB. All measurements took place at 25 °C with the following run parameters: a constant voltage of 250 V, 2.5 s on-time and 0.5 s off-time. The total run time was 60 s. The field direction was reversed and data were taken in both directions, to check on the consistency and reliability of the mobilities obtained.

2.3. Confocal microscopy and image analysis

The microscope measurements were carried out on a Leica SP2 CLSM. The CLSM was operated in fluorescence mode, with 488 nm excitation for the NBD dye and 543 nm for the RITC-labelled particles. The images were taken at low intensities (<200 μW) to make sure the light did not cause any decomposition of the solvent.

In the following we describe in more detail the conditions under which 3D data sets were taken to obtain the RDFs for the NBD-labelled PMMA spheres. Care was taken to ensure that the particles had not moved significantly during the time taken to scan a 3D image. The measured self-diffusion coefficient gave a Brownian time τ_B of 10 s for a particle to diffuse one diameter for fairly dilute fluids of the NBD–PMMA spheres, rising to 19 s for a fluid close to crystallization. In order to acquire images, the scan time had to be much less than τ_B. This was achieved by scanning 128 × 128 × 20 pixels, which took around 3 s. However, due to the finite size of the colloids, and the loss of image borders due to filtering, all the centres were sampled from a region of 112 × 112 × 12 pixels. Effectively, this reduces the scan time further, to around 2 s, since it is only the colloid centres that contribute to the RDF. The pixels had an xy spacing of 200 nm, and the separation between the xy planes was 600 nm. All images were acquired at least 10 μm from the wall of the capillary. We took care to ensure the sample was not bleached during imaging; up to 100 3D images were required to acquire enough statistics to produce an RDF. The time between successive 3D images was 30 s for concentrated regions, and at least 20 s for dilute regions. The lowest density data necessitated slightly different parameters: images of 256 × 256 × 32 pixels were scanned, the pixel size was again 200 nm in xy and 600 nm in z. As before, the colloid size and filtering effectively reduces this to 240 × 240 × 24 pixels. While the increased scan time of the larger images necessarily reduced the accuracy of the particle tracking, we note that the RDF histogram bins (see results section) are rather wider at this volume fraction (0.5σ, compared to 0.1σ at higher volume fractions), so the loss of accuracy is not expected to affect the results. At intermediate densities, the two scan sizes yielded the same result.

We adapted the method of Crocker and Grier [17] for 3D, and refined it to improve the handling of our somewhat noisy data. After a noise reduction step by Gaussian filtering, this method identifies particles by searching for pixels that are brighter than their neighbours. These are taken as trial centres. The intensity-weighted centroid of a circle centred on the brightest pixel of a radius equivalent to the colloid (or more accurately, the 2D convolution

of the colloid and a circle of the same size) is then taken as a better, sub-pixel, measure of the particle's geometric centre. This method is equally applicable to 3D images: one simply determines the local maximum in 3D and takes the centroid of an intensity-weighted sphere centred on the maximum to obtain the coordinates. There is some distortion in the z-direction due to the more limited resolution in the z-direction, so in the images the spheres are somewhat elongated. However, these particles are 2 μm in diameter, which is considerably larger than the 500 nm resolution in the z-direction, so in fact the elongation is not too severe and we argue that our use of spheres to sample a more accurate centroid is at least reasonable.

However, the method of Crocker and Grier suffers from two key shortcomings, in the case of noisy data. Firstly, there may be more than one local intensity maximum within the particle, leading to over-counting and erroneous RDF results. Here, multiple maxima found within one particle diameter were excluded, the brightest one being selected. Secondly, the brightest pixel may not lie near the geometric centre of the particle. This means the intensity-weighted centroid (which takes the brightest pixel as its centre) samples a different region from that of the particle, and arrives at an inaccurate value for the centre of the particle. We improved the accuracy by iterating the process: initially, the (intensity-weighted) centroid of near-neighbour pixels of the brightest pixel was found. This new centroid was then taken as the starting point to determine the centroid of next-nearest-neighbour pixels, which then gives a third estimate for the geometric centre of the particle. This is repeated out to the radius of the particle (in the case of this paper, 5 xy pixels). The whole process was then iterated ten times. In all tests, the algorithm converged on a stable solution within five iterations. The analysis was conducted in 3D, with appropriate scaling for the larger pixel size in the vertical direction.

The analysis described required two parameters: the minimum pixel intensity to be considered a local maximum, and the diameter for multiple centre exclusion. Throughout, we required that the results be insensitive to these parameters: the diameter was set to 10 pixels, and the minimum intensity was 128 (on a scale of 0–255). Care was taken to try to have maximum intensities to be close the 8 bit maximum value with which images were taken. Only tiny changes in the data resulted from varying the minimum intensity for maxima between 64 and 144, and the diameter between 8 and 12 xy pixels. The number of centres in a known volume gave the local colloid density. No density variations were found on the scale of the microscope images, despite the macroscopic density gradient. Nor were there any measurable density gradients introduced by diffusion during the time it took to perform the measurements.

The RDF, $g(r)$, is the probability of finding a pair of particles at a distance r apart, divided by the same probability for an uncorrelated system at the same density. Practically, this amounts to summing the pairs at each separation, and normalizing with a calculation for uncorrelated 'ideal gas' particles at the same density:

$$g(r) = \frac{\langle N(r, r+\delta r)\rangle}{N\rho V(r, r+\delta r)} \tag{1}$$

where $N(r, r+\delta r)$ is the number of particles lying in the range $r, r+\delta r$ from the test particle. N is the total number of particles, ρ is the number density and V is the volume of a spherical shell of thickness δr and inner radius r. Angled brackets denote a statistical average.

In an infinite system, the number of particles whose centres lie between $r, r+\delta r$ scales as r^2, the volume of a spherical shell of thickness δr. In a finite system, as r becomes comparable to the system size (here the microscope image) then much of the spherical shell lies outside the system. Correspondingly fewer points contribute to the numerator in equation (1). This can be resolved by sampling the denominator from a box of identical dimensions containing at least 10^4 uncorrelated coordinates (instead of a simple scaling as for infinite systems [18]). The effects of the finite size are simply 'divided out'. Since we scanned relatively quickly, with a separation of 600 nm between xy planes, our coordinates in the z-direction may be

comparatively inaccurate. We believe this should not greatly affect the RDFs. The aspect ratio of the region from which the coordinates are sampled is 0.3, so most interparticle separations have a greater component in the xy plane than in the z-direction. Therefore, an error in the z-direction then tends to act along the normal to the line connecting the particles, so the error in r in equation (1) is fairly small.

In the crystalline phase, only xy data were recorded. 512 images were collected, one every 1.6 s. The pixel size was 100 nm, and the images contained 512×512 pixels. Here, the same algorithm for coordinate finding as described above was used, except that it ran in 2D. The coordinates were then tracked in time using the algorithm of Crocker and Grier [17]. This yielded a complete history of each particle, although occasionally a particle might move far enough in the z-direction not to be tracked, so 1–2% of the time-series were incomplete.

In order to determine the excursions, the mean lattice position needed to be determined first. However, the lattice site of each particle was not known *a priori*, but was determined as follows. The centre of mass (COM) of the whole system was subtracted from the particle coordinates at each time, to remove any drift. The mean lattice sites were then taken as the time-averaged particle position with respect to the COM. We determined the probability of excursion as a function of distance, and found the effective potential well, $w(r)$, through $\beta w(r) = -\ln P(r)$, where $\beta = 1/k_{\mathrm{B}}T$, k_{B} is Boltzmann's constant, T the absolute temperature, and $P(r)$ the probability of an excursion of length r.

Weiss *et al* [19] showed that, for excursions within 10% of the lattice spacing, this effective potential well is harmonic,

$$\beta w(r) = \tfrac{1}{2}kr^2 \tag{2}$$

which defines an 'effective spring constant', k. We found our results to be well described by a harmonic potential well. By fitting equation (2) to our measurements, a value for k in both the x- and y-directions was determined.

2.4. Monte Carlo simulations

We used MC simulation in the canonical ensemble with periodic boundary conditions [18]. The MC acceptance ratio was constrained to lie in the range 0.4–0.5 by varying the steplength. The hard-core (HC) Yukawa potential from an approximate solution of the Poisson–Boltzmann equation was used throughout, with fixed parameters, $\kappa\sigma$ the ratio of the particle diameter σ and Debye length κ^{-1}, and $\beta\varepsilon$, the potential at contact in units of $k_{\mathrm{B}}T$, where k_{B} is Boltzmann's constant and T is the absolute temperature.

$$\beta u_{\mathrm{Yuk}}(r) = \begin{cases} \infty & r < \sigma \\ \beta\varepsilon \dfrac{\mathrm{e}^{-\kappa(r-\sigma)}}{r/\sigma} & r \geqslant \sigma \end{cases} \tag{3}$$

where $\beta\varepsilon$ is related to the effective colloid charge by

$$\beta\varepsilon = \frac{\beta Z^2 l_{\mathrm{B}}}{\sigma(1+\kappa\sigma/2)^2} \tag{4}$$

where Z is the effective colloid charge, [5]. l_{B} is the Bjerrum length

$$l_{\mathrm{B}} = \frac{\beta \mathrm{e}^2}{\varepsilon_{\mathrm{r}}\varepsilon_0} = \frac{\kappa^2}{4\pi c_{\mathrm{i}}}$$

where ε_{r} is the relative dielectric permittivity, ε_0 is the permittivity *in vacuo* and c_{i} is the concentration of monovalent ions.

The RDFs were calculated following the procedure described by Frenkel and Smit [18]. The system was allowed to equilibrate by requiring that the potential energy showed no more

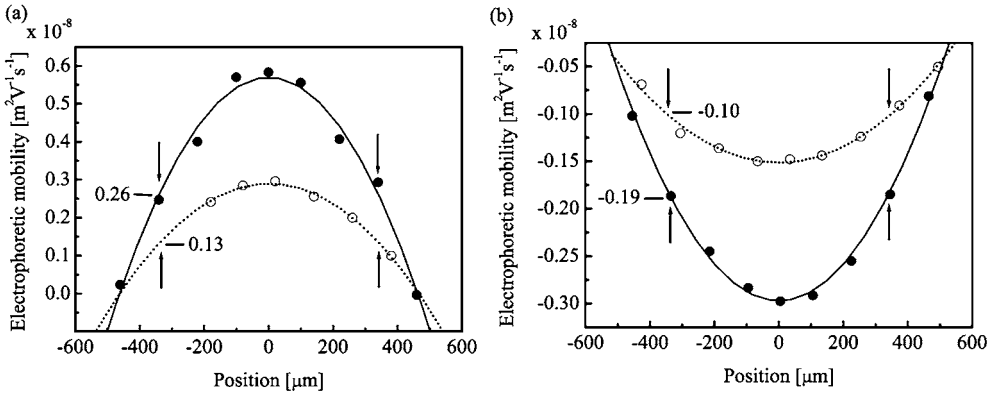

Figure 1. Electrophoretic mobility profiles. The rectangular capillary has a wall-to-wall distance of 1000 μm. The centre is at position 0 and the stationary layers are located at -340 and 340 μm (indicated by arrows). Open circles: 2.0 μm NBD–PMMA; solid circles: 2.16 μm RITC–PMMA. Parabolic fits to the measured profiles are drawn as curves. For each profile the value of the electrophoretic mobility at the stationary layer is given. The measurements were performed in a density-matching cyclohexyl bromide–hexane mixture, either (a) with no salt added or (b) with 40 μM TBAC (degree of dissociation $\sim$ 0.027).

than thermal fluctuations. Typically, this varied from 2×10^4 attempted MC moves for dilute fluids of 108 particles to 3.4×10^6 moves for crystals of 6912 particles. Data were sampled from at least 10^5 moves for fluids and 1.4×10^7 moves for crystals. For fluids, the system size was determined by requiring that the RDF was close to unity within half a box length. In the case of crystals, the 'effective spring constant' was found to show some sensitivity to system size. Increasing the size from 500 to 6912 particles changed the value by 6%. However, this effect became less pronounced at larger system sizes; from 2048 to 6912 the change was only 2%, tending towards a constant value for a large system.

The simulated excursions of the spheres around their lattice positions in the crystal were analysed in exactly the same way as the experimental data. That is to say, although the 'exact' mean lattice points were known, those used in the analysis were determined in the same way as described above for the experimental data.

3. Results and discussion

3.1. Mobility and conductivity

Despite the relatively low dielectric constant of the CHB–hexane solvent mixture used ($\varepsilon_r \sim 6.6$ when averaged over the volume for the different components in the mixture), we obtained mobility profiles that agree well with theory for electrophoretic flow in rectangular capillaries (figure 1). We fitted these profiles with second-order polynomials and calculated the electrophoretic mobility at the stationary layers [20]. The potential at the surface of shear (zeta potential) was then obtained via the O'Brien and White numerical scheme [21]. For the dispersions used here it can be safely assumed that the plane of shear more or less coincides with the particle surface so that the zeta potential reflects the value of the surface potential.

Dispersions without any added salt were found to have positive zeta potentials, +100 and +56 mV for RITC– and NBD–PMMA respectively. The conductivity of the purified CHB was 0.002 μS cm^{-1}, which corresponds to an ion concentration of 5.6×10^{-8} M (assuming

it to be a 1–1 electrolyte) and a value of 404 nm for κ^{-1} (these values for the pure CHB solvent are taken as an estimate for the CHB–hexane mixture). The addition of 40 μM TBAC (conductivity 0.045 μS cm^{-1}, ion concentration 1.0×10^{-6} M and $\kappa^{-1} \sim 94$ nm in pure CHB) resulted in smaller mobilities, which were now negative (figure 1). The corresponding surface potentials were calculated to be -98 mV for RITC–PMMA and -43 mV for NBD–PMMA. This salt-induced charge reversal of the particles was not mentioned in [4]. Real space, confocal microscopy studies of particle motion in a DC electric field supported our observations. In pure CHB, and in mixtures of this solvent with either *cis*-decalin or hexane, the PMMA particles carry a positive charge as well, and again the charge was reversed by the addition of (a sufficient amount of) TBAC.

At present, the mechanisms responsible for the charging and charge reversal are not known and are under investigation. Some results available now can narrow down the possibilities, however. Earlier studies [4] already pointed out that neither drying and/or distilling the solvent, nor the use of undyed particles had an effect on the softness of the potential. We confirmed these findings, as we only observed increased screening when adding water, whilst drying the dispersions with calcium chloride did not have any effect at all. PMMA systems with different dyes (including fluorescein isothiocyanate-labelled silica cores coated with a thick shell of unlabelled PMMA) and particles without dye display a similar positive charging behaviour. This excludes the dye as a possible source of the charge and also makes a direct role of water in the charging mechanism less likely. However, it is certainly possible that the *amount* of charge is modified by dye and/or water inside the PMMA spheres. The PHS–PMMA spheres have already been studied in quite a range of apolar solvent mixtures and, in fact, are used as a hard-sphere model system in many of these mixtures [22]. As far as we know, the occurrence of low volume fraction crystallization for the PHS stabilized PMMA system in these solvents has not yet been reported. Therefore, it is very likely that the origin of the charge is related to the CHB solvent. Alkyl halides are prone to self-decomposition; in CHB this would lead to the formation of HBr. Only a small amount of this gas dissolved in CHB, which has a relative dielectric constant of $\varepsilon_r = 7.9$, could already explain the background conductivity of 0.002 μS cm^{-1}. If the H^+ ion were to end up preferentially in the PMMA sphere it could also explain the positive particle charge. Apparently, after the addition of TBAC it is the Cl^- ion that preferentially ends up in the PMMA spheres, even to the extent that the surface charge is reversed, but we do not yet fully understand the chemical processes involved in this ion absorption. The fact that the surface charge can be controlled, however, makes this an even more interesting model system. Moreover, we are currently investigating whether combined additions of HBr and TBAC can control the surface charge (including the sign) *and* the electrolyte concentration independently.

3.2. Yukawa potential and Monte Carlo simulations

This section is divided into three parts. First we discuss the fluid phase, and the fitting of the RDFs obtained. Then we map our experimental results onto the theoretical phase diagram of point Yukawa particles [23]. Finally, we comment on the interparticle potential in the colloidal crystal phase as was inferred from an analysis of the particle excursions around lattice positions.

Confocal micrographs of the system at some of the state points sampled are shown in figure 2. All of these images were taken in the same capillary, showing that our centrifugation method is indeed capable of producing a density gradient that is stable over 24 h. The change from a disordered gas-like fluid, first to a dense, more ordered fluid and finally to a face-centred cubic (FCC) crystal is clear. There were no signs of the effects mentioned in section 3.3. Volume fractions were determined from the 3D particle tracking method described

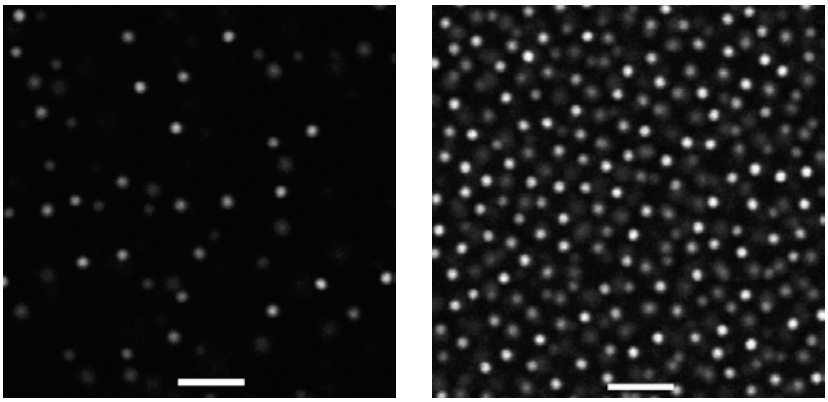

(a) $\eta = 0.01$ (b) $\eta = 0.058$

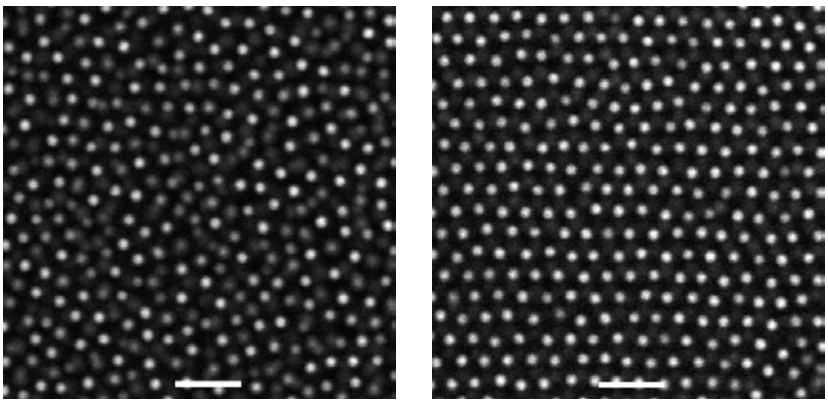

(c) $\eta = 0.094$ (d) $\eta = 0.101$

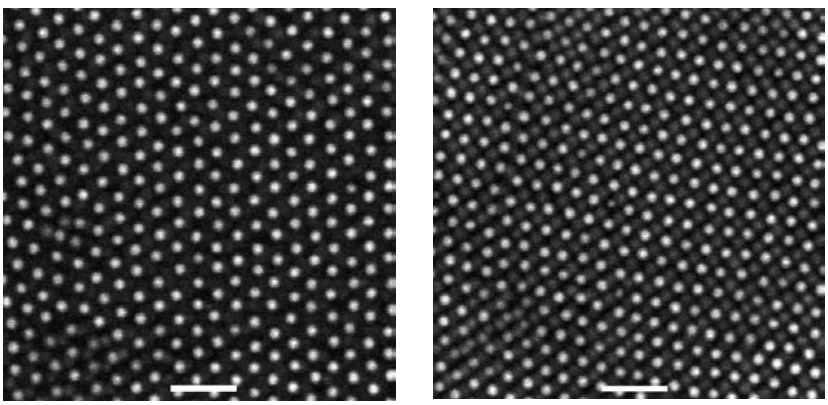

(e) $\eta = 0.121$ (f) $\eta = 0.171$

Figure 2. Confocal images of 2 μm NBD–PMMA spheres in density-matched CHB–decalin mixtures at various colloid densities, in the same capillary, at a depth of around 30 μm. Note the relatively low volume fractions of crystallization into FCC crystals between $\eta = 0.094$ and 0.101 compared to that of hard spheres (0.49) and the absence of the 'anomalous' effects described in section 2.3. The 'effective spring constant' was found for the crystal in (e). In (d) and (e) (111) FCC planes are visible, in (f) a (100) plane. Bars = 10 μm.

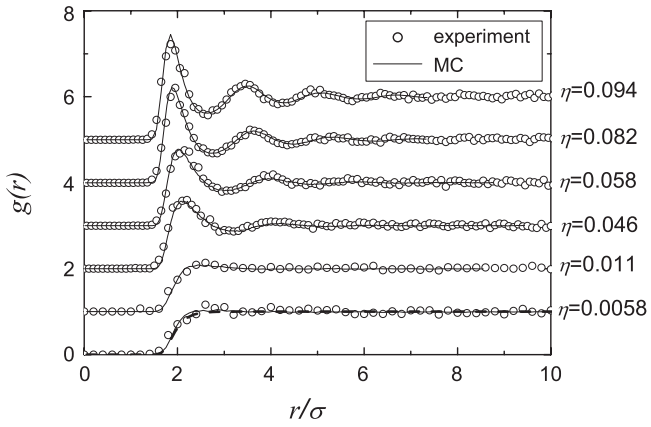

Figure 3. The RDF at various densities in the fluid phase of the system given in figure 1. The circles are experimental data. The solid curves are MC simulation data, with $\beta\varepsilon = 140$, $\kappa\sigma = 5$ at all densities. The dotted curve for $\eta = 0.0058$ is the 'Boltzmann relation' (equation (5)), valid for a dilute system.

in section 2.1. The sample was found to crystallize at a volume fraction between $\eta = 0.094$ and 0.101 ± 0.005. The error bound on the crystal volume fraction reflects the finite number of crystal planes in the sampled region. This relatively low volume fraction of crystallization compared to that of hard spheres (0.49) is a clear indication of the charged repulsions.

The RDF results are presented in figure 3. The experimental points are overlaid with solid curves from MC simulation results at corresponding densities. All the simulations took the parameters of $\beta\varepsilon = 140$, $\kappa\sigma = 5$ for the HC Yukawa potential. These parameters map to a effective colloid charge of 645 elementary charges and Debye length of 400 nm in this system. Our fitted value for the Debye length roughly corresponds to the background electrolyte concentration as determined by conductivity. The zeta potential was calculated to be 36 mV [20], in reasonable agreement with the electrophoresis result of 56 mV for a dispersion in pure CHB (the RDF samples were in nearly density-matched CHB–*cis*-decalin).

The slight difference in the height of the first peak of the RDF for $\eta = 0.094$ can be attributed to small inaccuracies in particle tracking. If we assume a normally distributed error in the particle coordinates, with a standard deviation of one pixel (0.1σ), and apply it to the 'exact' simulation data, to mimic the experimental results, the discrepancy disappears. The dotted curve for $\eta = 0.0058$ is the Boltzmann relation, valid in the dilute limit where only pairs of particles interact,

$$g(r)_{\eta\to 0} \approx \exp(-\beta u(r)). \tag{5}$$

The agreement between experiment, simulation and equation (5) suggests that, at this volume fraction, we are reasonably close to pair interactions.

There is agreement between the simulated and experimental RDFs, to within experimental error, suggesting that the effective pair-potential does not change appreciably as a function of colloid density. Therefore, we find no evidence for many-body effects, although cancellations between (for example) 3- and 4-body effects cannot be excluded. However, the work of Hynninen *et al* [14] suggests that, for $\kappa\sigma = 5$, and $\beta\varepsilon$ around 100, the effects of three-body interactions are small. We expect higher-order interactions to be still less important. Furthermore, Russ *et al* [13] calculated some four-body contributions, and found them to be attractive like the three-body effects, suggesting that cancellation of higher-order interactions

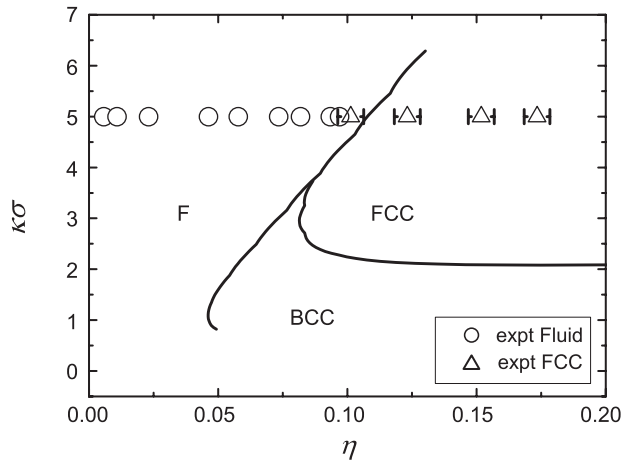

Figure 4. Experimental results mapped onto the theoretical phase diagram, for $\beta\varepsilon = 140$ [23]. F is fluid, FCC and BCC are face- and body-centred cubic crystals respectively. The black circles and triangles denote experimental fluids and FCC crystals.

may be unlikely. In the 2D work of Brunner *et al* [9], the colloids had a far higher effective charge, of the order of 10^4 elementary charges (at 5.2, their $\kappa\sigma$ was very close to that found here). Furthermore, the 2D system tended to suppress freezing, which meant that RDFs could be measured up to relatively higher densities, where many-body effects are more apparent. The agreement with a purely repulsive interparticle potential supports our earlier comment that there are no signs of interparticle attractions in these data sets.

Since we have a measure of the fluid–FCC phase boundary, and the pair-potential, we tried mapping the results onto a theoretical phase diagram determined for point Yukawa particles [23], see figure 4. The experiment maps out the constant $\kappa\sigma$ line of the phase diagram, for state points such as those shown in figure 2. There is good agreement with this theoretical phase diagram, and we found an FCC freezing volume fraction in agreement with theory. The theoretical phase diagram concerns point Yukawa particles, without an HC. However, since the contact value, $\beta\varepsilon$, is determined as 140, and does not fall to $k_{\mathrm{B}}T$ at until the particles are separated by 1.87σ, we argue that the cores almost never come into contact. Indeed simulated RDFs without the HC are indistinguishable from those with an HC. Hynninen and Dijkstra [24] have shown that, for these parameters, the HC has negligible impact on the phase behaviour.

For a check on the interparticle potential in the crystalline state close to melting, we analysed time-series of images such as figure 2(e), and analysed the excursions around the lattice points assuming a harmonic potential. The experiment gave a 'spring-constant' of $k_x = 60.7\sigma^{-2}$ and $k_y = 53.4\sigma^{-2}$. Here x and y refer to the horizontal and vertical directions in figure 2(e). This compares to $k = 58.73 \pm 0.38\sigma^{-2}$ for a simulation of 6912 particles with the same HC Yukawa potential, $\beta\varepsilon = 140$, $\kappa\sigma = 5$, as was found for the fluid. Here the simulation was carried out with the sides of the box in the FCC-100 orientation, so the Cartesian axes are equivalent: therefore we simply take an average for k. It appears that the FCC phase can also be described by the same HC Yukawa pair potential as the fluid phase, at least as far as $\eta = 0.121$.

To investigate the effect of crystal orientation, we conducted a smaller simulation of 576 particles in the FCC-111 plane, to match that of figure 2(e). Here we found values of $k_x = 62.04\sigma^{-2}$, $k_y = 61.78\sigma^{-2}$ and $k_z = 56.70\sigma^{-2}$. For comparison, an FCC-100 simulation

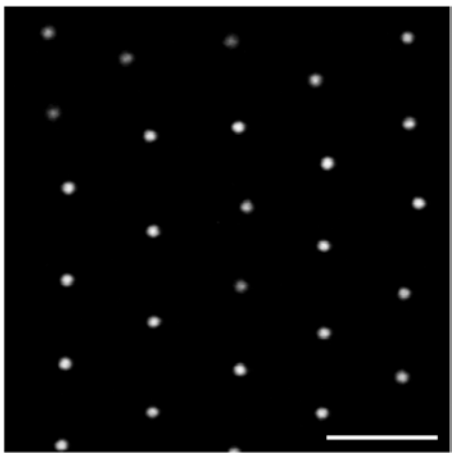

Figure 5. An extreme low-density crystal. A crystal of RITC-labelled particles in pure CHB. The interparticle spacing is $\sim$17 μm. The scalebar corresponds to 20 μm.

for a similar system size of 500 particles yielded $k = 63.14 \pm 0.9\sigma^{-2}$. This suggests that, for the parameters investigated here, the orientation is not too important. We have so far assumed perfect crystals in the simulations, despite the defects and distortions apparent in the experiment (figures 2(d)–(f)). Future work will include at least a simple treatment of defects.

Note that for the system used here, the background ion concentration of around 3×10^{-8} M is much larger than the concentration of counter ions coming from the surface charge. In addition, since 90% of the capillary is empty of colloids, there is an ion reservoir that gives these background ions a constant chemical potential and therefore makes the Debye screening length independent from the volume fraction of the colloids.

3.3. Anomalous (phase) behaviour

In the following we describe observations that were made fairly shortly (within a day) after dispersing dry particles in the solvent mixtures mentioned. It is important to remark that the observed phenomena were transient. After this transition period 'ordinary' phase behaviour as reported in section 3.2 was observed. Ordinary behaviour was obtained more quickly for higher salt concentrations and for dispersions that were grounded by ITO or wire electrodes placed in contact with the dispersions. We do want to report on the observed 'anomalous' behaviour, because it is very reminiscent of observations made by other groups in highly deionized dispersions in water [3, 7, 8]. We will discuss three different types of observations that are hard to explain with the pair potentials as determined in section 3.2: crystals at very low volume fractions, 'coexistence' of high and low density crystals, and voids.

Crystals with interparticle spacings up to 28 μm have been observed in the pure CHB solvent; see figure 5 and [4] for examples. The structure of these crystals is body-centred cubic, as expected for these soft spheres. However, the extremely low packing fractions (as low as 0.033%) do not agree with the measured zeta potentials and screening lengths of these dispersions. The background electrolyte concentration ($\sim 10^{-8}$ M) would give rise to much shorter screening lengths ($\sim$1 μm). Crystals with such extreme lattice spacings are observed over shorter timespans after preparation ($\sim$1 day) for smaller particles (diameter 1 μm) and tend to exist longer for particles with a size of 2 μm ($\sim$days); with 4 μm sized spheres they can even persist for weeks.

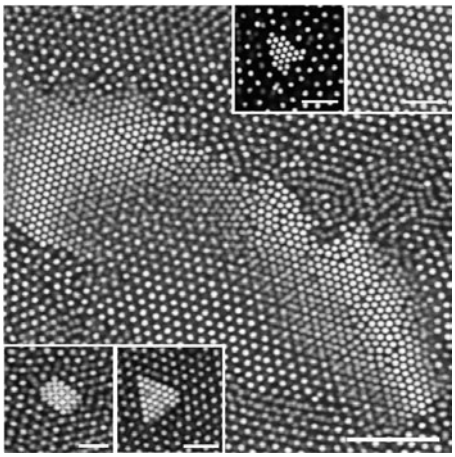

Figure 6. High-volume fraction crystals in the presence of low-volume fraction structures. Several 'anomalous' nuclei of NBD-labelled particles. The big nucleus is partly covered by the surrounding lower density material. The scalebar in the main image corresponds to 25 μm, the ones in the insets to 10 μm.

Another instance of anomalous behaviour is the spontaneous formation of compact structures, which we will refer to as 'nuclei'. These pieces of crystalline material consist of tens to thousands of particles and have a very small interparticle spacing, only a little larger than the particle diameter (2.00 μm), e.g. 2.05 μm for the big nucleus depicted in the main image of figure 6, and 2.10 μm in the top right-hand inset. Surrounding them is a colloidal gas/fluid or a crystalline lattice with the same symmetry, but a much larger spacing. The structures are three-dimensional, often consisting of multiple layers. Although the nuclei appear rapidly, within minutes to days, we never saw any growth after their initial formation. We made sure the structures are not 'dried-in' aggregates that fell back into the dispersion.

Finally, we also occasionally encountered 'voids', irregularly shaped regions in the colloidal fluid or crystalline lattice with only a few particles present inside (figure 7). The voids were observed to extend over several hundreds of micrometres. Near the voids, the surrounding lattice is disordered. The particles at the edges are quite mobile, but there is no or only very slow diffusion inside the voids. These structures appear within minutes to weeks and can be very long-lived (up to weeks).

Although we never saw material besides the colloids in the confocal microscopy images we had the idea the voids could be related to foreign inclusions, such as pieces of polymer, present in the dispersion. To test this hypothesis we intentionally added pieces of foreign material to the dispersions in CHB. With small pieces of metal we were able to induce the formation of structures that resemble the voids: see figure 8. We added the small pieces of metal wire (tens of micrometres or less) to freshly prepared dispersions and placed them in a sonic bath for a couple of minutes, before filling the sample capillary.

On the surface of the metal pieces the structure of the colloids is irregular, caused by the large van der Waals forces, but a little further away the colloidal structure is crystalline with the lattice spacing increasing with the distance to the surface. Further away, there are also regions in between and underneath these 'crystals' that are void of particles. These 'holes' behaved in a similar way to the voids described earlier on and depicted in figure 7.

Both the crystals and the holes move around; their positions and translations are correlated. The holes are sharply bounded, but they nevertheless are dynamic structures. They change

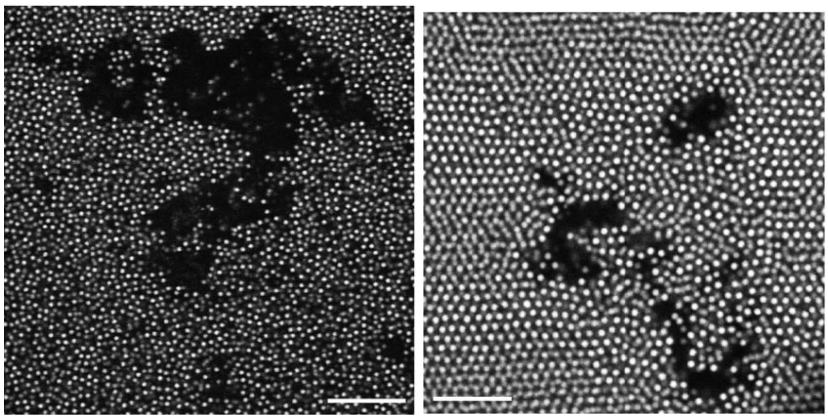

(a) (b)

Figure 7. Voids. Extensive, three-dimensional voids are surrounded by (a) a colloidal fluid or (b) a crystalline lattice of NBD–PMMA particles. The scalebars correspond to 30 and 20 μm respectively.

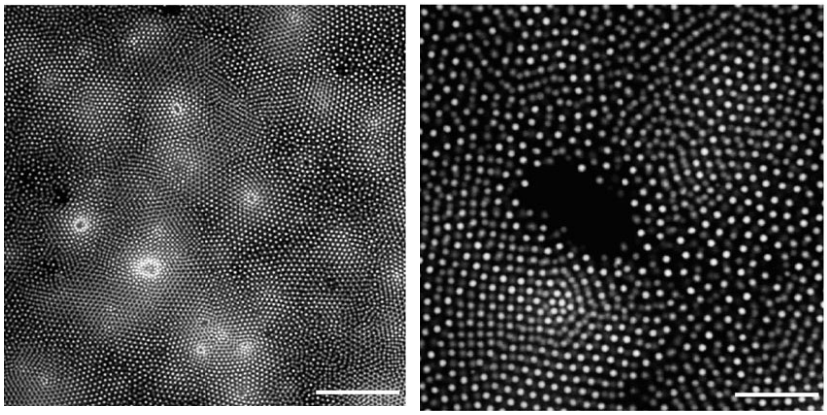

(a) (b)

Figure 8. The effects of added pieces of metal. Both images are of NBD–PMMA spheres in pure CHB. (a) The pieces of metal, intentionally introduced to the system, are visible as dark spots surrounded by a high density of particles. They induce crystallization and smaller interparticle spacings close to the metal. The scalebar corresponds to 50 μm. (b) A crystalline region is accompanied by a three-dimensional empty hole/void somewhat further away. The scalebar corresponds to 20 μm.

position, size and shape roughly following the motion of the metal pieces. The dynamics of the few particles that we observed inside some of the holes is noticeably different from that of the surrounding fluid. In general, the crystals and the holes are long-lived structures; it takes hours to relax to a homogeneous colloidal fluid. Grounding the cell, however, speeds up this relaxation process, whilst the addition of salt to the dispersions suppresses all of the effects described.

As stated before, our observations are similar to observations made in highly deionized systems (see [11] for reviews on the subject). In particular we want to mention the reentrant

phase behaviour [7], the voids [6] and the long-lived metastable high-density crystals [8]. Because our system does not rely on ion-exchange resin to obtain low concentrations of ions, it is a welcome new system in which this 'anomalous' behaviour (in the sense of purely repulsive pair potentials) can be studied. Many possible explanations have already been brought forward [11], but one we are currently investigating and which has, as far as we know, not yet been mentioned is that these effects may be caused by excess charge present in the dispersion. Excess charge in the literal sense: (initially) there is no charge neutrality in the dispersion. This charge can then end up on (intentionally added) foreign material or any impurities present in the dispersion, possibly giving rise to voids; otherwise it can reside on the colloids themselves, which may be the cause of the crystals with extremely large interparticle spacing. Eventually, the system relaxes to electroneutrality in the equilibrium situation by a charge flow to or from earth. Such excess charges could be induced by flow, for example when filling the capillaries or making the dispersions. In low-conductivity media the build-up of charges by these processes has been investigated because of the hazards the resulting fields can cause in the petroleum industry [25]. Conductivities in CHB are low, but still large enough so that they would discharge a capacitor in milliseconds. We are currently investigating the relaxation time and the influence on the interparticle interactions if the excess charge is located on the colloids themselves.

4. Conclusions

We have shown that with dye-labelled and sterically stabilized PMMA spheres dispersed in a mixture of CHB and *cis*-decalin, 3D coordinates and RDFs for a colloidal fluid can be obtained with confocal microscopy. As far as we know, this has not been reported before. The fact that we did not use a fast scanning confocal microscope, such as a Nipkov disc system, suggests that significant improvements in signal to noise and scan rate are still possible. The use of centrifugation in an almost density-matched dispersion created a sample with a constant chemical potential of the background ions and a large range of volume fractions that could be probed in a single capillary. The background electrolyte concentration for the 3D RDF study, 10^{-8} M, was an order of magnitude lower than can be obtained in water. However, this background concentration was still much higher than the counter-ion concentration. The colloidal size was larger than the double layer thickness. All this taken together explains why both the structure in the colloidal liquid, the crystallization volume fraction and the restoring forces towards the lattice positions in the colloidal crystal could all be well described with a (pairwise) Yukawa potential that did not depend on density. The absence of indications for many-body effects is in keeping with the work of [14] for our HC Yukawa parameters of $\beta\varepsilon = 140$ and $\kappa\sigma = 5$. Many-body effects would be more apparent in a system with a longer Debye screening length and/or much higher effective colloid charge [9]. We plan to investigate this range in a follow-up study both with optical tweezers and determination of RDFs. Electrophoresis measurements showed that the salt TBAC can be used to change the Debye screening length *and* can cause a charge inversion from positive to negative.

Anomalous behaviour, i.e., from a point of view of pair-wise additive repulsive potentials, was observed relatively shortly after the dispersions were made and was mostly transient. The behaviour was either absent or changed more quickly for smaller particles, grounded dispersions and higher salt concentrations. Our observations included extremely long-range repulsions, 'coexistence' of high-density and low-density colloidal crystals, and void formation. Previously these kinds of phenomena have been reported for deionized dispersions in water [6–8]. As our model system is different in many aspects from the aqueous systems, there are new chances for finding an explanation for these strange phenomena. Specifically,

we are presently investigating the possibility of excess charge residing on the PMMA colloids shortly after making the dispersions.

Acknowledgments

We thank A Yethiraj and A D Hollingsworth for discussions and for performing some of the conductivity measurements, and A-P Hynninen, S Williams, M Dijkstra and R van Roij for helpful discussions. This work is part of the research program of the Stichting voor Fundamenteel Onderzoek der Materie (FOM), which is supported by Nederlandse Organisatie voor Wetenschappelijk Onderzoek (NWO).

References

[1] van Blaaderen A and Wiltzius P 1995 *Science* **270** 1177–9
[2] Kegel W K and van Blaaderen A 2000 *Science* **290–293** 287
[3] Gasser U, Weeks E R, Schofield A, Pusey P N and Weitz D A 2001 *Science* **292** 258–62
[4] Yethiraj A and van Blaaderen A 2003 *Nature* **421** 513–6
[5] Overbeek J and Verwey E J 1949 *Theory of the Stability of Lyphobic Colloids* (Amsterdam: Elsevier)
[6] Ito K, Yoshida H and Ise N 1994 *Science* **263** 66–8
[7] Arora T B, Tata B V R, Sood A K and Kesavamoorthy R 1988 *Phys. Rev. Lett.* **60** 2438–41
[8] Larsen A E and Grier D G 1997 *Nature* **235** 230–3
[9] Brunner M, Bechinger C, Strepp W, Lobaskin V and von Grunberg H H 2002 *Europhys. Lett.* **58** 926–32
[10] Brunner M, Bechinger C and von Gruenberg H H 2003 Direct measurement of three-body interactions in colloidal suspensions *J. Phys.: Condens. Matter* **15**
[11] Tata B V R and Arora A K 1996 *Ordering and Phase Transitions in Colloidal Systems* (New York: VCH)
[12] van Roij R, Dijkstra M and Hansen J P 1999 *Phys. Rev.* E **59** 2010–25
[13] Russ C, von Grunberg H H, Dijkstra M and van Roij R 2002 *Phys. Rev.* E **66** 011402
[14] Hynninen A-P, van Roij R and Dijkstra M 2003 Effect of triplet interactions on the phase diagram of suspensions of charged colloids *J. Phys.: Condens. Matter* **15**
[15] Antl L, Goodwin J, Hill R, Ottewill R and Waters J 1986 *J. Colloids Surf.* **17** 67–78
[16] Bosma G, Pathmamanoharan C, de Hoog E H A, Kegel W K, van Blaaderen A and Lekkerkerker H N W 2002 *J. Colloid Interface Sci.* **245** 292–300
[17] Crocker J C and Grier D 1996 *J. Colloid Interface Sci.* **179** 298–310
[18] Frenkel D and Smit B 2001 *Understanding Molecular Simulation: from Algorithms to Applications* (New York: Academic)
[19] Weiss J A, Larsen A and Grier D G 1998 *J. Chem. Phys.* **109** 8659–66
[20] Hunter R J 1981 *Zeta Potential in Colloid Science* (London: Academic)
[21] O'Brien R W and White L R 1978 *Faraday Trans.* II **74** 1607–26
[22] Pusey P N and van Megen W 1986 *Nature* **320** 340–2
[23] Hamaguchi S, Farouki R T and Dubin D H E 1997 *Phys. Rev.* E **56** 4671–82
[24] Hynninen A-P and Dijkstra M 2003 *Phys. Rev.* E **68** 021407
[25] Klinkenberg A and van der Minne J L 1958 *Electrostatics in the Petroleum Industry* (Amsterdam: Elsevier)